Research paper

Evaluation of atmospheric corrections on hyperspectral data with special reference to mineral mapping

Nisha Rani [a], Venkata Ravibabu Mandla [b,*], Tejpal Singh [c]

[a] Centre for Disaster Mitigation and Management (CDMM), VIT University, Vellore, India
[b] OSGST-Lab, Department of Environmental, Water Resources Engineering, School of Civil and Chemical Engineering, VIT University, Vellore, India
[c] CSIR-Central Scientific Instruments Organisation, Chandigarh, India

ARTICLE INFO

ABSTRACT

Hyperspectral images have wide applications in the fields of geology, mineral exploration, agriculture, forestry and environmental studies etc. due to their narrow band width with numerous channels. However, these images commonly suffer from atmospheric effects, thereby limiting their use. In such a situation, atmospheric correction becomes a necessary pre-requisite for any further processing and accurate interpretation of spectra of different surface materials/objects. In the present study, two very advance atmospheric approaches i.e. QUAC and FLAASH have been applied on the hyperspectral remote sensing imagery. The spectra of vegetation, man-made structure and different minerals from the Gadag area of Karnataka, were extracted from the raw image and also from the QUAC and FLAASH corrected images. These spectra were compared among themselves and also with the existing USGS and JHU spectral library. FLAASH is rigorous atmospheric algorithm and requires various parameters to perform but it has capability to compensate the effects of atmospheric absorption. These absorption curves in any spectra play an important role in identification of the compositions. Therefore, the presence of unwanted absorption features can lead to wrong interpretation and identification of mineral composition. FLAASH also has an advantage of spectral polishing which provides smooth spectral curves which helps in accurate identification of composition of minerals. Therefore, this study recommends that FLAASH is better than QUAC for atmospheric correction and correct interpretation and identification of composition of any object or minerals.

1. Introduction

Solar radiation scattered from the Earth's surface interacts with atmosphere before reaching to any space-based or airborne remote sensing sensor. The atmospheric interaction (mainly absorption and scattering) affects the actual radiance recorded for any given point on the ground. However, the magnitude of absorption and scattering varies spatially and temporally depending on the nature and concentration of various atmospheric constituents (Gao and Goetz, 1990). Earth's atmosphere contains CO_2, O_2, O_3, H_2O, CH_4, CO, NH_4, N_2O and other gases which interact with approximately half of the electromagnetic radiation (EMR) spectrum over the wavelength region from 0.3–2.8 μm (Gao and Goetz, 1990; Gao et al., 1993). Major atmospheric water bands are centered at approximately 0.94, 1.14, and 1.88 μm (Gao et al., 2006). The oxygen band is at 0.76 μm and the carbon dioxide band is near 2.08 μm. Therefore, about half of the 0.4–2.5 μm spectral region is affected by atmospheric gas absorption (Gao et al., 2006). In particular, regions of the EMR spectrum, such as 0.9, 1.1, 1.4 and 1.9 μm are almost opaque to remote sensing sensors (Lau, 2004). Therefore, regions that do not contain significant absorption features are called transmission windows. These transmission widows are exploited by remote sensing sensors. However, these also suffer from atmospheric effects that need to be suitably corrected for better interpretation.

Recently, space based hyperspectral images have found wide use in mineral mapping and lithological discrimination in various geological units (Kruse et al., 2003; Rowan et al., 2004; Hubbard and Crowley, 2005; Van Ruitenbeek et al., 2006; San, 2008). These images have the advantage of narrow band widths with

* Corresponding author.
E-mail address: ravi.mandla@vit.ac.in (V.R. Mandla).

Peer-review under responsibility of China University of Geosciences (Beijing).

numerous channels that hold much more information than conventional multispectral images, about any area of investigation and therefore are better suited for geological studies i.e. mineral mapping and lithological discrimination. These images have wide applications in other fields also which include agriculture, forestry and environmental studies etc. However, as mentioned above these images commonly suffer from atmospheric effects and rarely depict the true radiance of the surface (Adams and Gillespie, 2006), thereby limiting their direct use. In such a situation, atmospheric correction becomes a necessary pre-requisite to any further processing and accurate interpretation of hyperspectral images. It is also required for radiance to reflectance conversion (Goetz et al., 2002). During the atmospheric correction, raw radiance data is re-scaled to reflectance data, shifting all spectra to nearly the same albedo. This permits comparison of reflectance spectra of image with the spectra of laboratory and field spectra, directly.

The spectral signatures play an important role in the identification of composition of any material on the Earth's surface. The study of spectral signature is known as spectroscopy or reflectance spectroscopy, where it derives information of any object by using wavelength range from the visible through, near infrared and shortwave infrared region (Clark, 1999). According to Clark (1995, 1999), spectroscopy may be described as the study of light, emitted, scattered or reflected from a gas, solid or liquid, as a function of its wavelength. When light interacts with any material at certain wavelength, some lights are preferentially absorbed while other wavelengths are transmitted. Thus, spectra of the sample or a continuous reflectance spectrum is obtained in the measured wavelength region (Van der Meer and De Jong, 2001). The absorption features in these spectra play a vital role for identification of their chemical or mineralogical compositions. The spectral reflectance in the visible and near-infrared (VNIR) region offers a rapid and inexpensive technique for determining the mineralogy of samples and obtaining information on their chemical composition. In this paper authors have tried to compare two different approaches of atmospheric corrections i.e. QUAC (Quick Atmospheric Correction) and FLAASH (Fast Line-of-sight Atmospheric Analysis of Spectral Hypercubes) for the spectra of vegetation, man-made structures and rock exposure with special reference to different minerals from Gadag area of Karnataka, India.
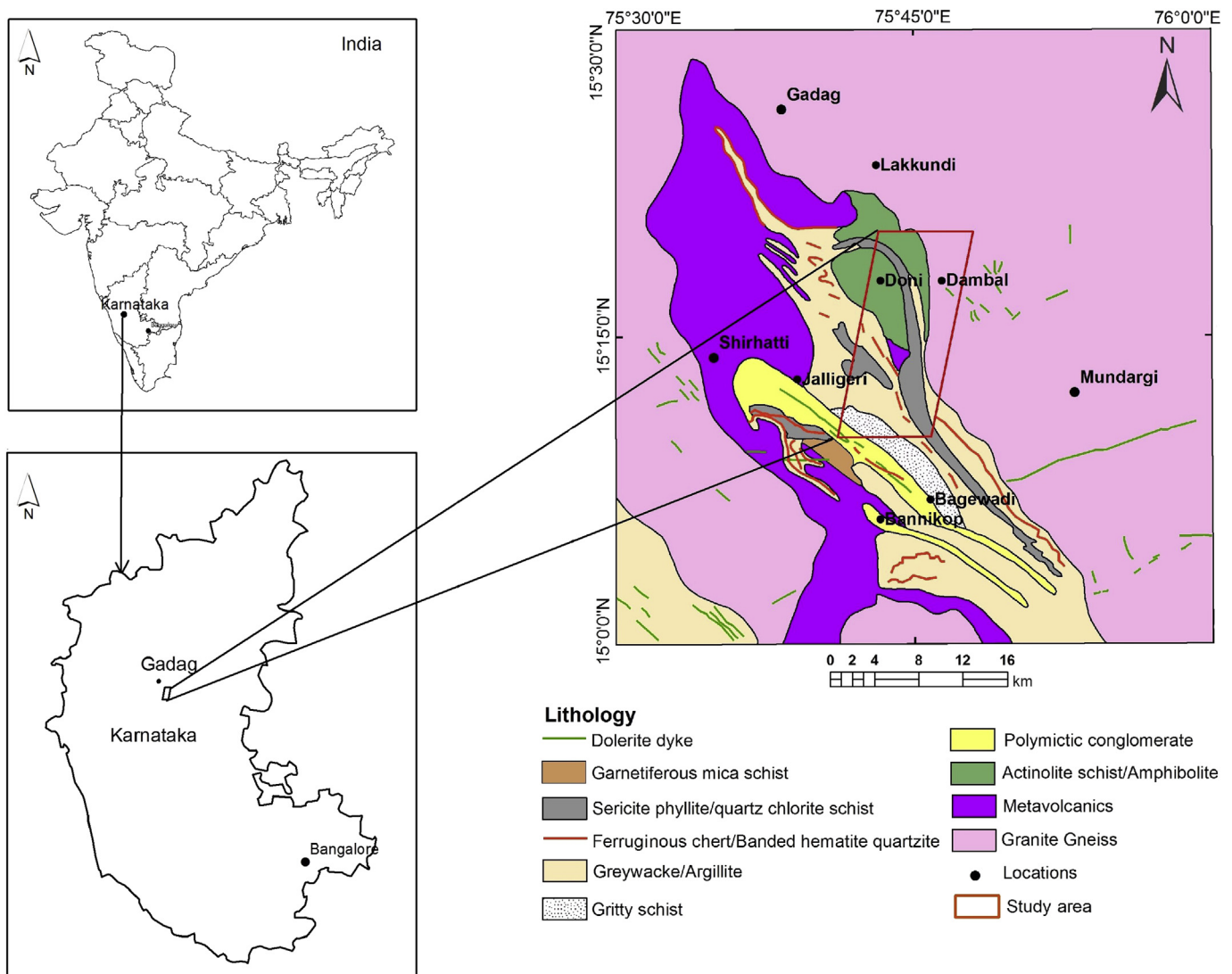

Figure 1. Geological map showing various lithological units of the study area. The red parallelogram shows coverage of the Hyperion data.

Table 1
Stratigraphic succession of Gadag schist belt (Beeraiah and Sengupta, 1998).

Quartz vein, Gabbro, dolerite intrusives, gray granite, pink granite, quartz porphyry		Post-tectonic	
Sericite phyllite, garnetiferous mica schist	Hiriyur Formation	Chitradurga Group	Dharwar Supergroup
Banded ferruginous chert			
Banded maganiferous chert			
Limestone			
Polymict conglomerate			
Metabasalt			
Argillite-chlorite phyllite			
Grit-greywacke			
Para-amphibolite			
Metabasics	Ingaldhal Formation		
Metavolcanics (massive, schistose, pillowed and vesicular basalts, acid volcanics, agglomerate)			
————————————————————————————Unconformity————————————————————————			
Gneissic/gneissic granite	Peninsular Gneissic Complex		
Ultramafics	Sargur Group		

2. Study area

The study area is located in the Western Dharwar Craton, south-east of Gadag, Karnataka (Fig. 1). The choice of the area is primarily due to the presence of good rock exposures with continuous mineralized zones (Deb, 2014; Rani et al., 2015). The choice of the study area is also limited by the availability of the hyperspectral image. Here, the Dharwar Craton is a well exposed granite-greenstone terrane that forms the basement (Glorie et al., 2014). It is endowed by considerable gold mineralization (Deb, 2014). The area exposes Peninsular Gneissic Complex (PGC) and an assemblage of volcano-sedimentary suite of rocks. The volcano-sedimentary rocks belong to Chitradurga Group of Dharwar Supergroup of Archaean to lower Proterozoic age that are intruded by dolerite dykes of lower Proterozoic age (Fig. 1).

In the study area, ultramafics of the Sargur Group are the oldest rocks whereas the quartz veins are the youngest rock unit (Table 1). The area is known as Gadag schist belt (GSB) and trends NNW–SSE with strike length of 50 km and maximum width of 22 km. The schist belt consists of metavolcanics with limestones, banded ferruginous chert and conglomerate. The intrusive phases in the belt are represented by quartz porphyries, sills and dykes of gabbro and dolerite and quartz veins. The schist belt is bounded in north-east and south-west by gneisses and granites (Chakrabarti et al., 2006). Greywackes and polymictic conglomerates are the most abundant sedimentary rocks in Gadag schist belt (Table 1, Fig. 1). They are inter-banded with subordinate cherts, banded iron formations and rare dolomitic limestone. Among the volcanic rocks basaltic and andesitic varieties predominate. The contact between the gneissic rocks and the rocks of the schist belt is generally sharp, at places it is marked by quartz-feldspathic veining; in some others the contact appears to be faulted (Chakrabarti et al., 2006). The metavolcanic rocks dominate in the western part whereas actinolite schist and sericite phyllite are predominant in the eastern part of the belt (Fig. 1). The polymictic conglomerate, gritty schist and garnetiferous mica schist occur extensively in the core of the synform (Fig. 1).

3. Data and methods

In the study hyperspectral remote sensing data (EO1H1450492013085110KZ_1GST) procured through the United States Geological Survey (USGS) was used (Fig. 2). The Level 1 GST is radiometrically corrected, resampled for geometric correction. The 1GST image is ortho-corrected using digital elevation models (DEM) to correct parallax error resulting from local topographic relief (Kurt, 2006). The image used in the study belongs to path '145' and row '049' and was acquired on the 85th Julian day of the year '2013'.

Each image contains data for a 7.65 km wide (cross-track) and 185 km long (along-track) region. The image consists of 30 m × 30 m pixels, in which the spectrum for each portion is
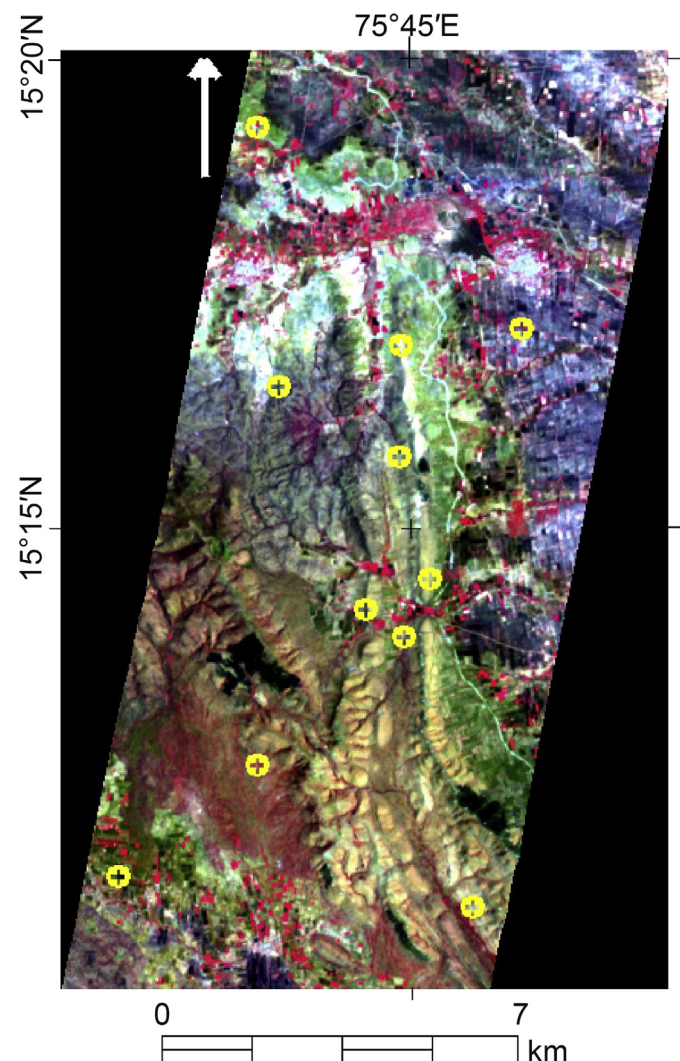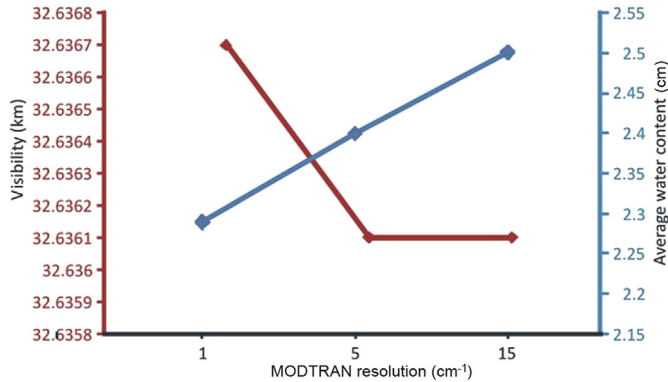

Figure 2. Geocoded hyperspectral image with locations of different spectra.

Table 2
Various parameters used in the FLAASH correction.

Site Center Latitude	15.22°N
Site Center Longitude	75.74°E
Acquisition date	2013-08-05
Sensor altitude	705 km
Ground elevation	850 m
Atmospheric model	Tropical
Sensor type	Hyperion
Pixel size	30 m
Aerosol scale height	2 km
Initial visibility	40 km

Figure 3. Variation of visibility and average water content for different MODTRAN resolutions.

provided (Beck, 2003). The data have 242 spectral bands ranging from 400–2500 nm, at approximately 10 nm spectral resolution and 30 m spatial resolution from a 705 km orbit (Beck, 2003). Only 198 out of 242 bands are calibrated. The calibrated channels 8–57

Table 3
The visibility and average water content.

Sr. no.	MODTRAN resolution	Visibility (km)	Average water content (cm)
1	1	32.6367	2.2896
2	5	32.6361	2.3989
3	15	32.6361	2.4998

for VNIR and 77–224 for the SWIR. The reason for not calibrating all 242 channels is mainly due to the detector's low responsivity (Beck, 2003). Further, due to an overlap between VNIR bands 56 (915.23 nm) and 57 (925.41 nm) and SWIR bands 77 (912.45 nm) and 78 (922.4 nm), only 196 unique channels are available for investigation (Beck, 2003; USGS, 2004). Scaling factor of 40 for spectral bands 1–70 (VNIR) and 80 for spectral bands 71–242 (SWIR) is applied to the calibrated radiance [$W/(m^2 \cdot sr \cdot \mu m)$]. Further, to obtain data units of $mW/(cm^2 \cdot sr \cdot \mu m)$, the data is factored by 10^{-1} (Barry, 2001).
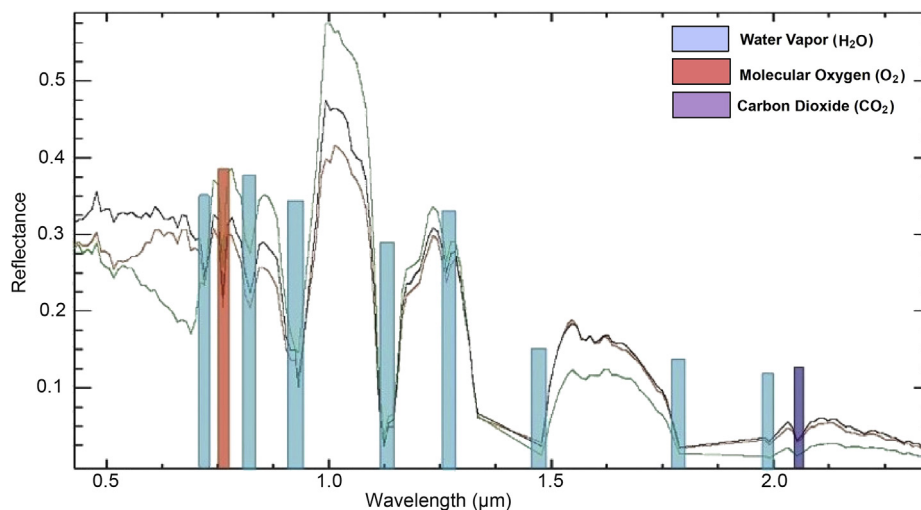
$$VNIR \times L = DN/40$$

$$SWIR \times L = DN/80$$

4. Atmospheric correction

Hyperspectral remote sensing is an advanced tool for research and applications in a variety of fields which include geology, agriculture, forestry and environmental studies etc. In order to use hyperspectral data to study surface properties, accurate removal of atmospheric effects is required. There is a need to correct for atmospheric effects and conversion of radiances measured by the sensors to reflectance of surface materials (Gao et al., 2006). Quantitative analysis of surface reflectance, therefore, mandates removal of atmospheric effects. Therefore, atmospheric correction forms an integral and necessary preprocessing step. The retrieved surface-reflectance spectra can then be compared directly with laboratory or field spectra representing different materials for their identification and classification. However, any such comparisons shall be beyond the scope, i.e. comparing approaches to atmospheric correction, of the current study.

There are basically two approaches: (1) empirical approach that is scene-based, and (2) model approach that is based mainly on radiative transfer model (Guo and Zeng, 2012). There are numerous algorithms available for both the approaches. However, we choose to use the most recent and advanced algorithms for them i.e. QUAC and FLAASH. QUAC is used for empirical approach and FLAASH for model approach. Each atmospheric approach is discussed in detail separately in the following paragraphs.

Figure 4. Absorption bands of atmospheric gases between 0.4 and 2.5 μm in the spectra of human settlement (black), rock exposure (red) and vegetation (green) generated from raw Hyperion data.
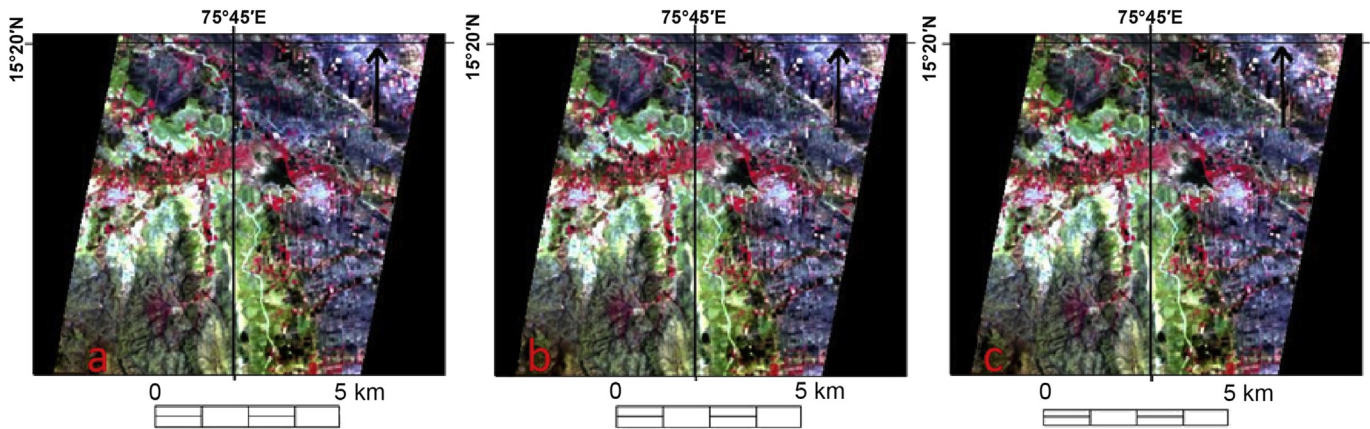
Figure 5. (a) Radiance image (raw), (b) QUAC corrected image, (c) FLAASH corrected image.
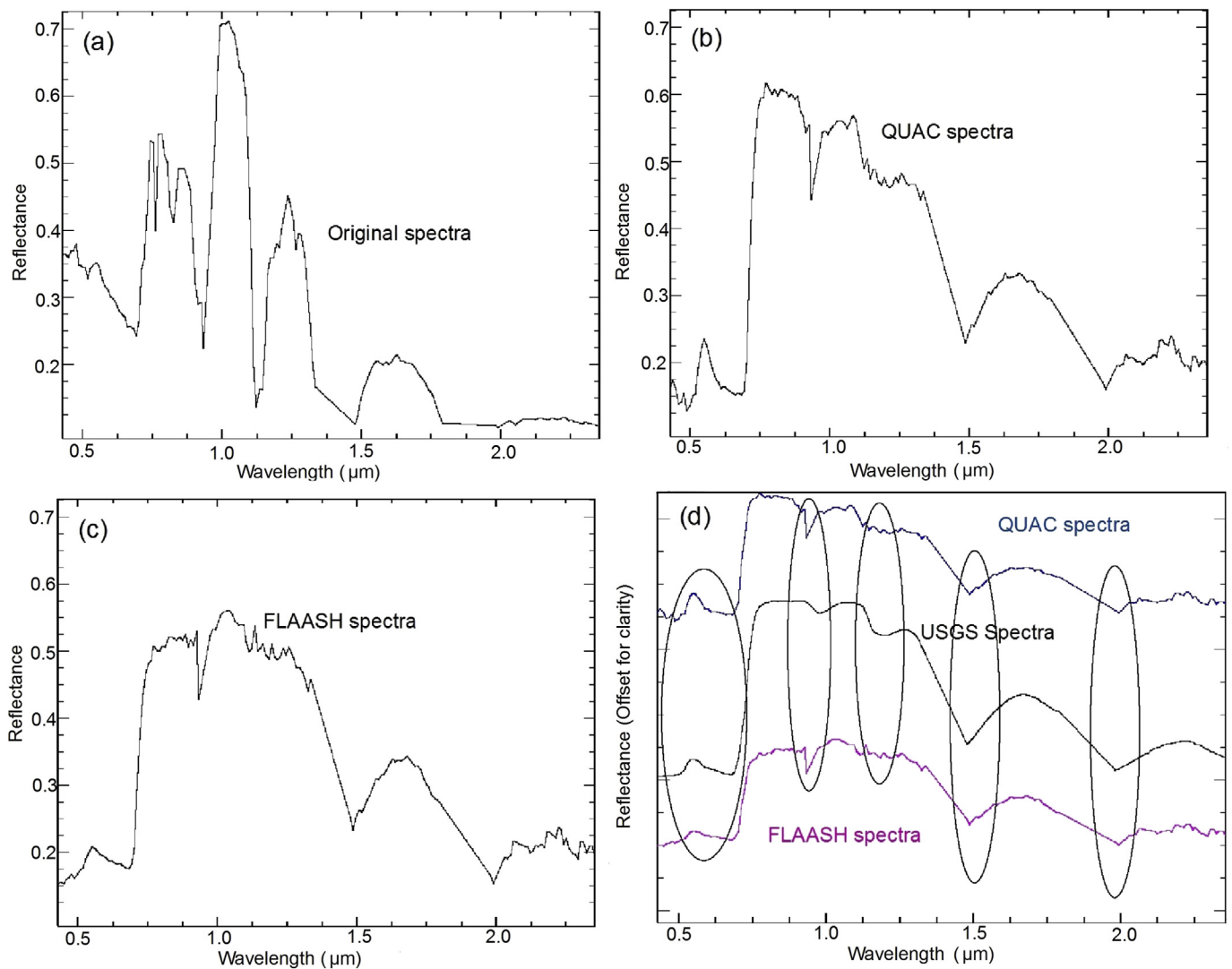

Figure 6. (a) Vegetation spectra of raw image, (b) vegetation spectra of QUAC corrected image, (c) vegetation spectra of FLAASH corrected image and (d) comparison of vegetation spectra of QUAC corrected (blue) and FLAASH corrected (magenta) image with spectra of USGS (black).

4.1. QUAC

Empirical approach depends highly upon the image information and usually does not require any field measurements. The QUAC algorithm works based on the diverse spectra in the image i.e. end members. However, it needs sufficient dark pixels in the scene to estimate the baseline spectra. This determines atmospheric compensation parameters directly from the information contained within the scene (observed pixel spectra), without ancillary information. It is based on the empirical findings that the average reflectance of a collection of diverse material spectra, such as the end member spectra in a scene (Agrawal et al., 2011; Guo and Zeng, 2012; Rani et al., 2015).

4.2. Model approach (FLAASH)

Most models based methods follow radiative transfer model (Gao and Goetz, 1990). FLAASH is most advanced besides the other models as it also accounts for adjacency effects (Adler-Golden et al., 1999). FLAASH is a first-principles atmospheric correction tool that corrects wavelengths in the visible through near-infrared and a shortwave infrared region, up to 3 μm. It incorporates the MODTRAN4 radiation transfer code (Agrawal et al., 2011; Guo and Zeng, 2012; Rani et al., 2015). The input image for FLAASH must be a radiometrically calibrated radiance image. Other information such as flight date, start time, time in GMT, scene center location, sensor altitude, and ground elevation is also required for this correction (Table 2).
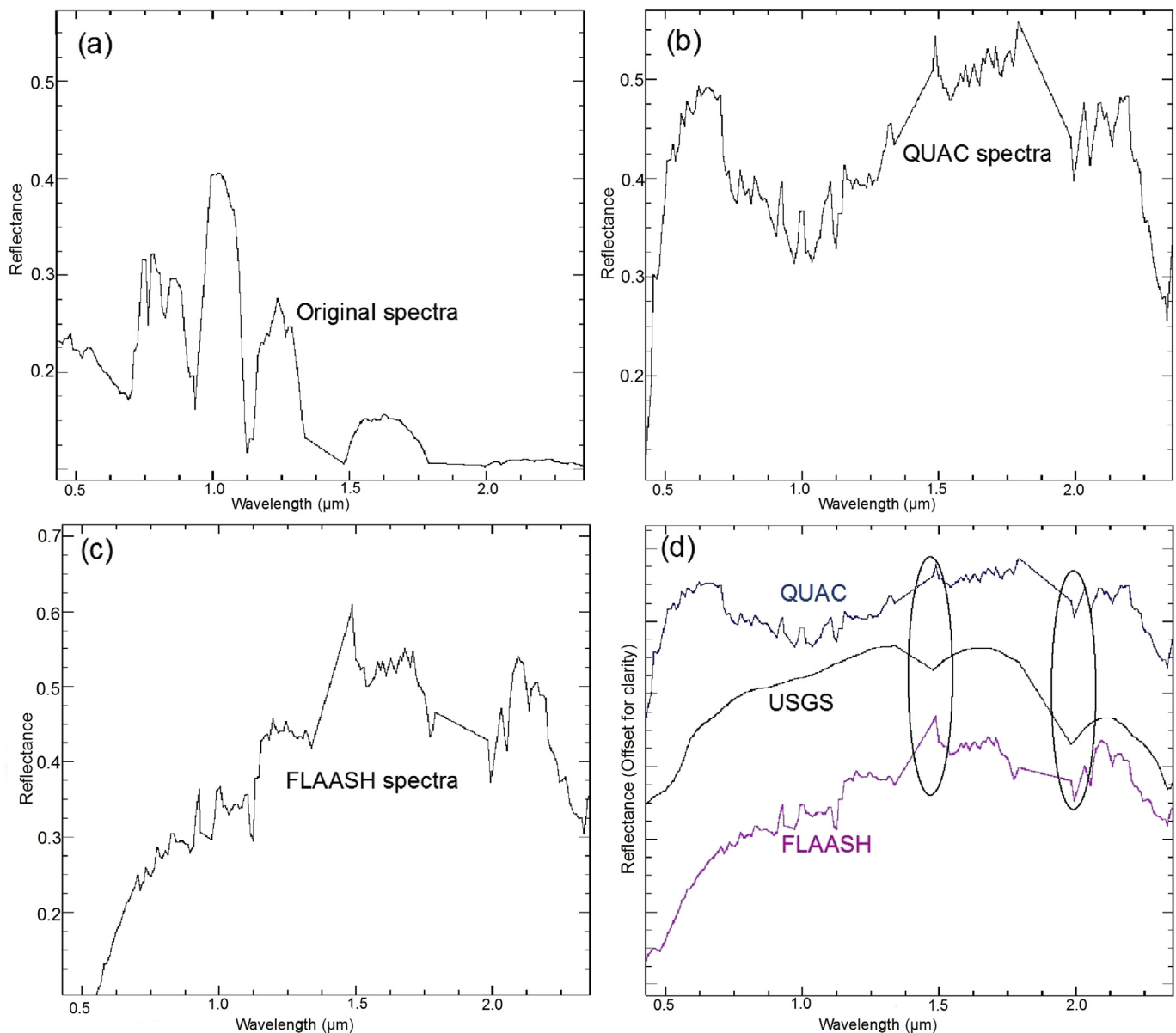

Figure 7. (a) Man-made structure spectra of raw image, (b) man-made structure spectra of QUAC corrected image, (c) man-made structure spectra of FLAASH corrected image and (d) comparison of man-made structure spectra of QUAC corrected (blue) and FLAASH corrected (magenta) image with spectra of JHU (black).

Before proceeding to atmospheric correction of the hyperspectral remote sensing data, pre-processing of the image is required. Pre-processing includes conversion of data format into BIL (Band interleaved format), removal of bad or uncalibrated and overlapped bands and resizing of bands. Bad band removal was carried out manually by visualizing each band. In all, out of a total of 242 bands, only 155 bands were considered for further processing.

Now, on the hyperspectral data containing 155 bands, QUAC atmospheric algorithm was applied. This requires only sensor type as the input parameter. It determines atmospheric compensation parameters directly from the information contained within the scene (observed pixel spectra), without any ancillary information.

Next, FLAASH atmospheric correction was also applied on the hyperspectral image. It is a rigorous method, which requires many parameters (Table 2). While applying FLAASH algorithm, scale factor is specified at the same time when the input radiance is specified. For the present study, the atmospheric model selected is tropical and aerosol model is rural. Aerosol retrieval function is turned on and the recommended 1135 nm feature is selected. The initial value for visibility is set to 40 km. The spectral polishing

option has been tested with the width for polishing operator set to 9. The IFOV value for Hyperion is 0.043. The aerosol scale height and CO_2 mixing ratio is 2.0 km and 390 ppm, respectively. The MODTRAN resolution 1, 5 and 15 were applied. The results of all three MODTRAN resolution 1, 5 and 15 and visibility show that for all the three MODTRAN the visibility remains almost same whereas the average water content shows conspicuous increase (Fig. 3 and Table 3).

5. Results and discussion

Prior to applying atmospheric correction algorithms on hyperspectral data, spectral signatures of the vegetation, man-made structure and rock exposures are captured. These spectra show major absorption at 0.69, 0.73, 0.76, 0.82, 0.94, 1.12, 1.2, 1.4, 1.7, 1.88, 1.9 and 2.0 μm (Fig. 4).

After applying atmospheric corrections on the hyperspectral remote sensing data, the results of original raw image, QUAC and FLAASH corrected images were evaluated and compared (Fig. 5a–c). Visual analysis shows that there is no significant
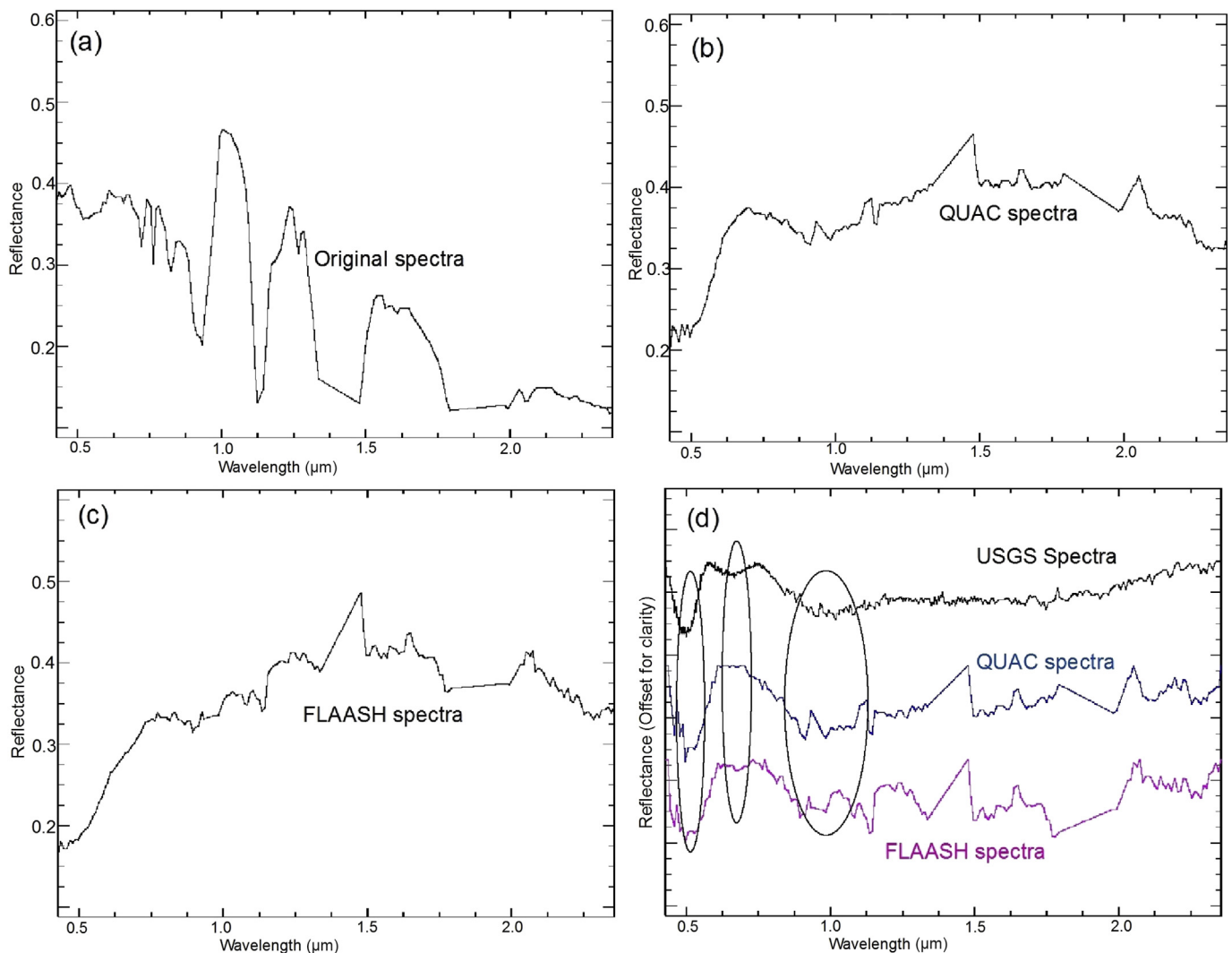

Figure 8. (a) Rock exposure (goethite) spectra of raw image, (b) rock exposure (goethite) spectra of QUAC corrected image, (c) rock exposure (goethite) spectra of FLAASH corrected image and (d) comparison of rock exposure (goethite) spectra of QUAC corrected (blue) and FLAASH corrected (magenta) image with spectra of USGS (black).

difference in these three images (raw, QUAC and FLAASH). Therefore, there is an urgent need to study the spectral signatures pertaining to each of the features in three images i.e. vegetation, man-made structures and rock exposures with special focus on different mineral spectra. The spectral signatures of different surface materials were generated from raw, QUAC and FLAASH corrected hyperspectral image (Fig. 2).

5.1. Vegetation spectra

Spectral signatures of vegetation were generated from the raw (radiance), QUAC and FLAASH corrected images (Fig. 6a−c). The spectral signature of the raw data shows prominent absorption from VNIR to SWIR region (Fig. 6a). These are attributed to strong absorption by atmospheric gases. As all vegetation contain some basic constituents, e.g. chlorophyll and other light-absorbing pigments, water, proteins, starches, waxes and structural biochemical molecules such as lignin and cellulose (Elvidge, 1990). These constituents contribute to absorption. Here, there is a substantial difference in the spectra of raw, QUAC and FLAASH corrected images

(Fig. 6). Spectra from QUAC and FLAASH were compared with each other and results indicate that spectra from both images show similarity in their absorption features (Fig. 6d). Strong absorption at 0.46 and 0.68 μm is due to the pigments in vegetation. Weak absorption at 0.98 and 1.2 is due to the presence of water in leaves. Strong absorption at 1.4 and 1.9 μm in both the spectra is due to water present in the vegetation. These spectra were also compared with vegetation spectra of USGS library and it is observed that the two spectra of atmospherically (QUAC and FLAASH) corrected hyperspectral image shows good correlation with spectra of USGS library (Fig. 6d).

5.2. Spectra of man-made structures

Spectra of man-made structures depend on many factors such as material used for building, age of the structure, weathering etc. The spectra of man-made structure collected from the raw image, shows absorption at 0.72, 0.76, 0.82, 0.93, 1.1, 1.2, 1.4, 1.9 and 2.0 μm (Fig. 7a). Spectra of the same locations were also collected for QUAC and FLAASH corrected images (Fig. 7b, c). It is observed that
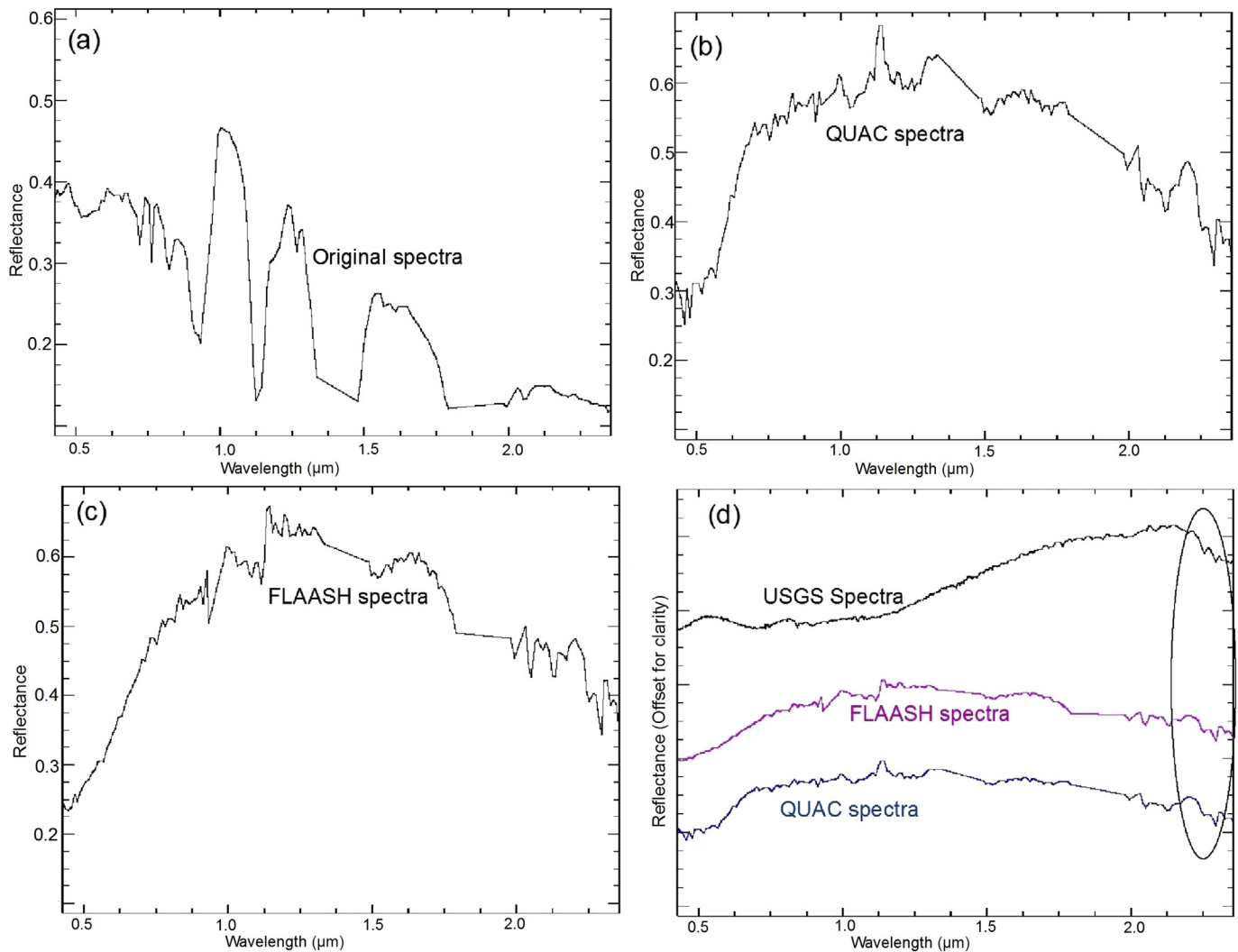

Figure 9. (a) Rock exposure (prochlorite) spectra of raw image, (b) rock exposure (prochlorite) spectra of QUAC corrected image, (c) rock exposure (prochlorite) spectra of FLAASH corrected image and (d) comparison of rock exposure (prochlorite) spectra of QUAC corrected (blue) and FLAASH corrected (magenta) image with spectra of USGS (black).

absorption of atmospheric gases was compensated in both the spectra. Further the spectra show a good match with the spectra of concrete material (courtesy: John Hopkin's University (JHU) library). It can be clearly seen that at 1.4 and 1.9 μm both algorithms (QUAC and FLAASH) have over estimated the atmospheric gas absorption.

5.3. Rock exposure spectra

The absorption caused in VNIR region (0.3 to 1.0 μm) is useful for mapping gossans rich in iron oxides and weathered sulphide occurrences such as hematite, jarosite, goethite etc. (Papp and Cudahy, 2002). The SWIR region is potentially useful for mapping alteration minerals which are largely related to the combination tones and overtones of vibrations of octahedrally coordinated cations such as Al, Mg, Fe, Si, CO_3, NH_4, and SO_4 bonded with hydroxyl (OH) group and carbonates (Hunt, 1979; Papp and Cudahy, 2002; Clark et al., 2007). Most minerals have a characteristic spectrum and diagnostic absorption features between the wavelength ranges of 1.3 to 2.5 μm (SWIR) (Meer et al., 2012).

The absorption of light in any rock exposure depends on the mineral composition of the rock, grain size, weathering pattern and bonding in the crystals of the mineral. Slight change in the mineral composition of the rock can change the character of absorption features. The spectral signatures of different rock exposures were captured in order to evaluate the atmospheric correction on the spectra of different minerals. These spectral signatures were compared with the USGS mineral library to identify the mineral compositions. Based on the similarity in the absorption features, following minerals were identified: goethite, prochlorite, kaosmec, hornblende and kaolinite.

Spectral signature of goethite was captured from raw, QUAC and FLAASH corrected images (Fig. 8a–c). Spectra of QUAC and FLAASH corrected images were compared with mineral library of USGS (Fig. 8d) and it shows that the absorption at 0.5 and 0.7 μm are well compensated in both the models. Absorption at 0.95 μm is compensated in FLAASH and over estimated in QUAC.

The spectra of prochlorite, which is a mineral of chlorite group, was captured from raw and atmospherically corrected images (Fig. 9c). QUAC and FLAASH spectra show diagnostic absorption at 2.25 and 2.35 μm, attributed due to presence of Al-OH and Mg-OH. The effect of atmospheric absorption is accurately compensated in both QUAC and FLAASH corrected images (Fig. 9d).
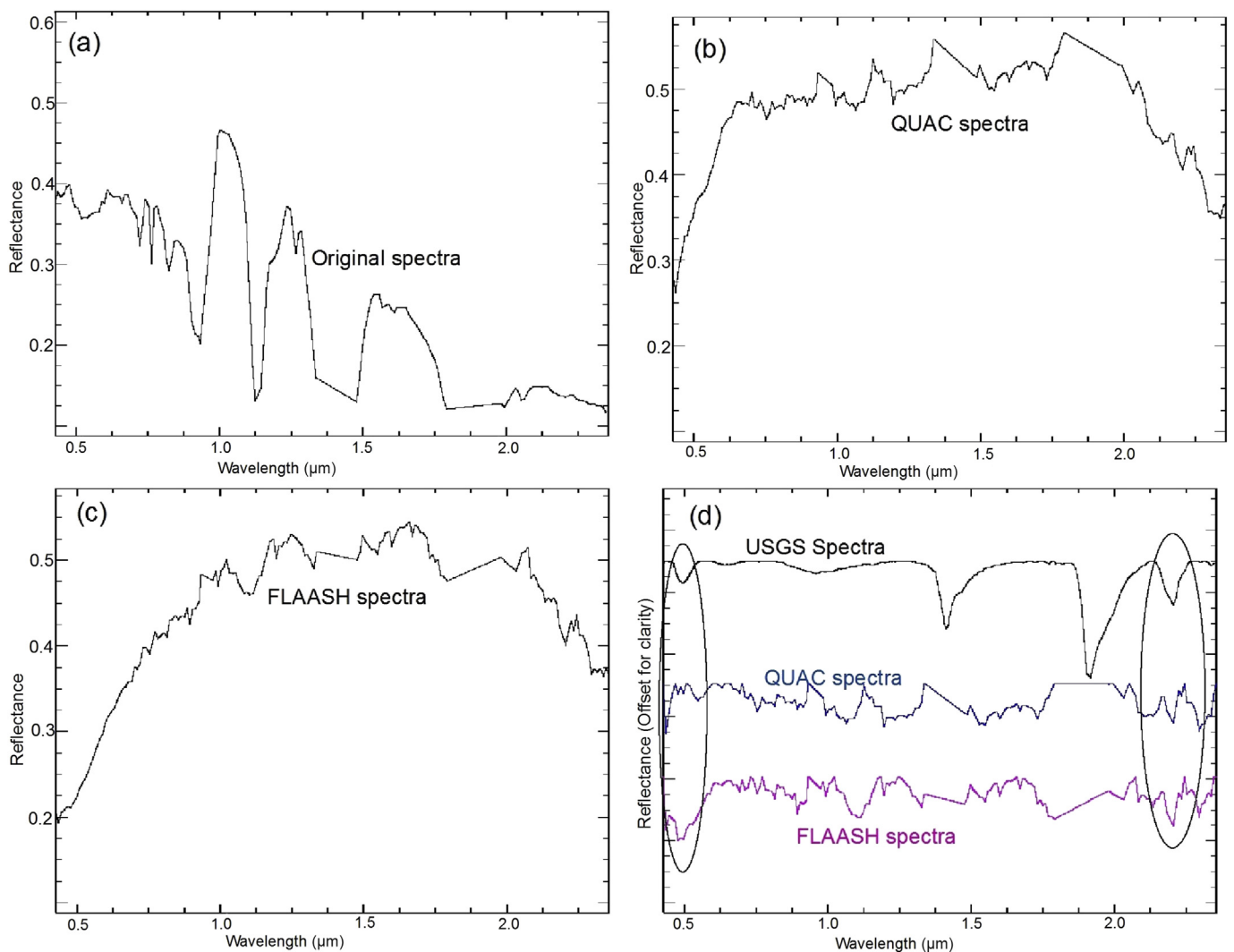

Figure 10. (a) Rock exposure (kaosmec) spectra of raw image, (b) rock exposure (kaosmec) spectra of QUAC corrected image, (c) rock exposure (kaosmec) spectra of FLAASH corrected image and (d) comparison of rock exposure (kaosmec) spectra of QUAC corrected (blue) and FLAASH corrected (magenta) image with spectra of USGS (black).
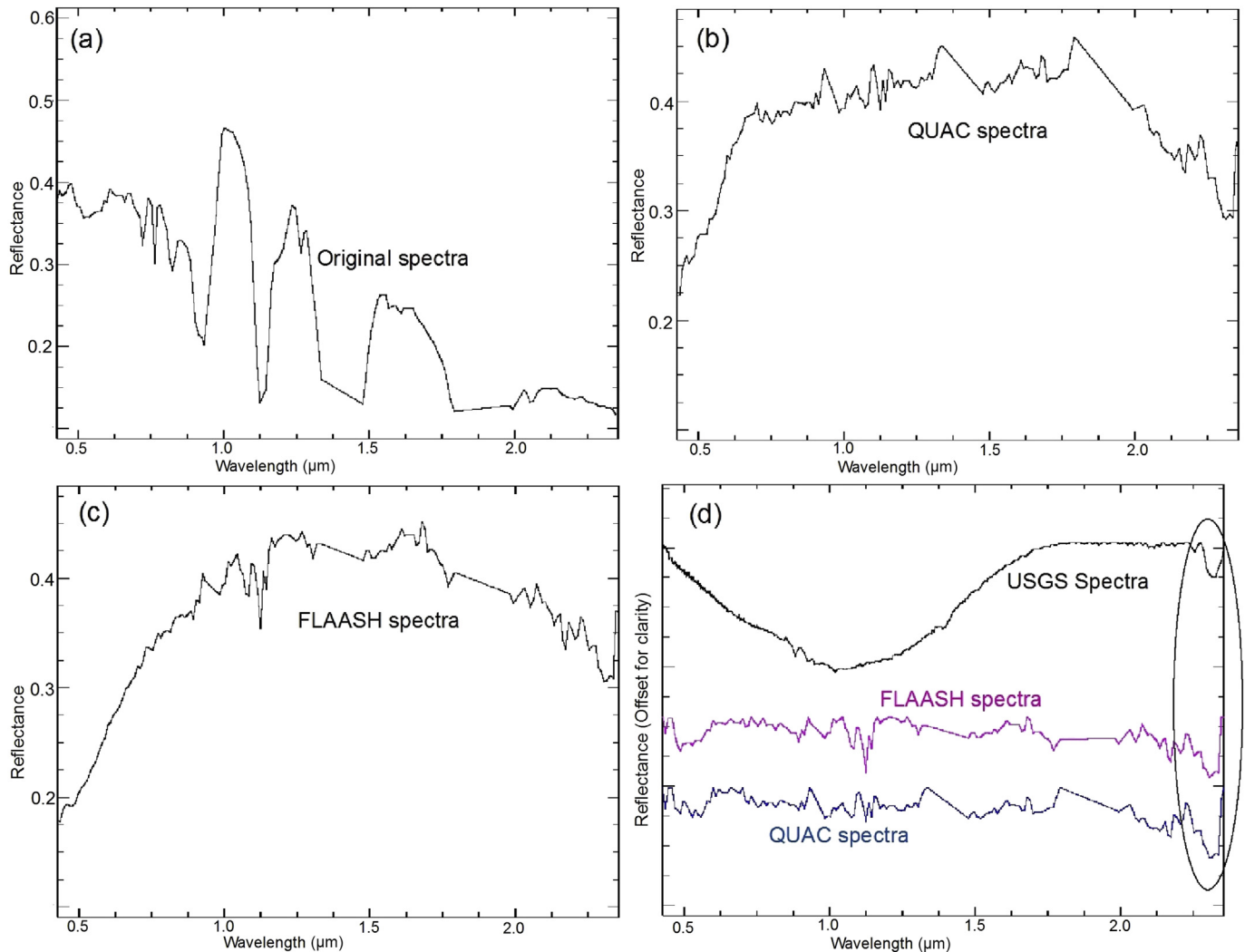
Figure 11. (a) Rock exposure (hornblende) spectra of raw image, (b) rock exposure (hornblende) spectra of QUAC corrected image, (c) rock exposure (hornblende) spectra of FLAASH corrected image and (d) comparison of rock exposure (hornblende) spectra of QUAC corrected (blue) and FLAASH corrected (magenta) image with spectra of USGS (black).

Similarly, the spectra of koasmec mineral from raw, QUAC and FLAASH corrected images were captured (Fig. 10a–c). Koasmec contains both kaolinite and smectite and shows diagnostic absorption at 2.2 μm. The effects of atmospheric absorption are compensated by both models (Fig. 10d).

Spectral signatures for hornblende and kaolinite were generated from raw, QUAC and FLAASH corrected images (Figs. 11a–c and 12a–c). The spectral analysis of hornblende shows characteristic absorption features at 2.32 and 2.39 μm. QUAC and FLAASH compensated this effect of atmospheric absorption (Fig. 11d). Kaolinite shows a sharp doublet near 2.1 and 2.21 μm due to the presence of both Mg and Al and their bonding with OH. It is a diagnostic absorption feature. The spectra were well compensated in QUAC and FLAASH models for atmospheric effects in both spectra (Fig. 12d).

6. Conclusions

Atmospheric correction is an important pre-requisite step to enhance and improve identification of spectral signatures of different objects or materials and their compositions. Spectra from raw image contain many absorption features which are contributed by the presence of gases and water vapor in the atmosphere. We explored the QUAC and FLAASH models to remove effect of absorption of atmospheric gases and water vapor. Also, individual spectra generated from hyperspectral data were compared directly with laboratory or field spectra. Based on the present investigation and comparison of raw, QUAC and FLAASH corrected spectral signatures following conclusions can be drawn:

(1) For vegetation, atmospheric absorption by gases and water vapor is well compensated by both algorithms. The corrected spectra match well with the spectra of USGS vegetation library. Strong absorption at 0.46 and 0.68 μm is due to the pigments in vegetation. Presence of water shows strong absorption at 1.4 and 1.9 μm and weaker at 0.98 and 1.2 μm.

(2) In the case of man-made structures, both models over estimate at 1.4 μm and compensate at 1.9 μm. These spectra are comparable to the ones from the JHU library and are identified as concrete material.

(3) The spectral signatures of different rock exposures reveal that FLAASH provides better result compared to QUAC. The spectra are well compensated for the effect of gases and water vapor.
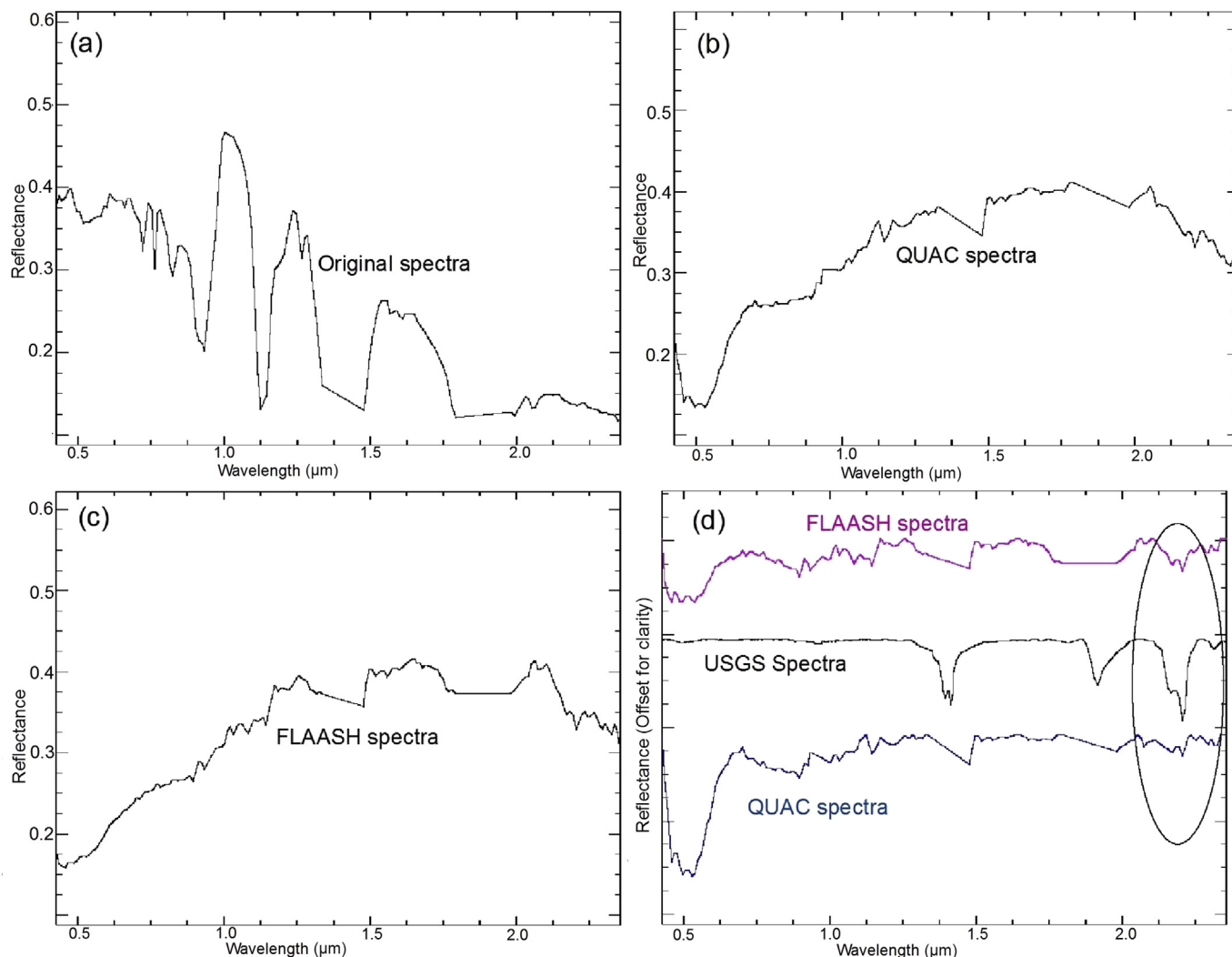
Figure 12. (a) Rock exposure (kaolinite) spectra of raw image, (b) rock exposure (kaolinite) spectra of QUAC corrected image, (c) rock exposure (kaolinite) spectra of FLAASH corrected image and (d) comparison of rock exposure (kaolinite) spectra of QUAC corrected (blue) and FLAASH corrected (magenta) image with spectra of USGS (black).

Overall, it appears that FLAASH is a rigorous atmospheric correction model that requires various parameters to perform but it has capability to compensate the effect of atmospheric absorption. It has an additional advantage of spectral polishing which provides smooth spectral curve. However, in absence of the aforesaid parameters QUAC can be used to obtain reasonably better results.

Acknowledgements

References

Adams, J.B., Gillespie, A.R., 2006. Remote Sensing of Landscapes with Spectral Images: A Physical Modeling Approach. Cambridge University Press, Cambridge, p. 362.

Adler-Golden, S.M., Berk, A., Bernstein, L.S., Richtsmeie, R.S., Acharya, P.K., Matthew, M.W., Aderson, G.P., Allred, C., Jeong, L., Chetwynd, J.H., 1999. FLAASH a MODTRAN4 atmospheric correction package for hyperspectral data retrieval and simulations. In: Proceeding 7th Annual JPL Airborne Earth Science Workshop, 97—21. JPL Publication, Pasadena, Calif., pp. 9—14

Agrawal, G., Sarup, J., Bhopal, M., 2011. Comparison of QUAC and FLAASH atmospheric correction modules on EO-1 Hyperion data of Sanchi. International Journal of Advanced Engineering Sciences and Technologies 4, 178—186.

Barry, P., 2001. EO-1/Hyperion Science Data User's Guide, Level 1-B.

Beck, R., 2003. EO-1 User Guide, Version 2.

Beeraiah, M.B., Sengupta, S., 1998. A Report on the Investigation for Gold in Malasamudra North Block, Gadag Schist Belt, Dharwar District, Karnataka.

Chakrabarti, D., Mallic, T.C., Pyne, T.K., Guha, D., 2006. A Manual of the Geology of the India. In: Precambrian, Part I-Southern Part of the Peninsula, fourth ed., vol. I, (Special publication no. 77).

Clark, R.N., 1995. Reflectance Spectra. American Geophysical Union, pp. 178—187.

Clark, R.N., 1999. Spectroscopy of rocks and minerals and principles of spectroscopy. In: Rencz, A.N. (Ed.), Remote Sensing for the Earth Sciences, Manual of Remote Sensing, third ed. John Wiley and Sons, New York, pp. 3—58.

Clark, R.N., Swayze, G.A., Wise, R., Livo, E., Hoefen, T., Kokaly, R., Sutley, S.J., 2007. USGS Digital Spectral Library splib06a: U.S. Geological Survey, Digital Data Series 231.

Deb, M., 2014. Precambrian geodynamics and metallogeny of the Indian shield. Ore Geology Reviews 57, 1—28.

Elvidge, D.E., 1990. Visible and near infrared reflectance characteristics of dry plant materials. Remote Sensing of Environment 11, 1775—1795.

Gao, B.C., Goetz, A.F., 1990. Column atmospheric water vapour and vegetation liquid water retrievals from airborne imaging spectrometer data. Journal of Geophysical Research 95 (D4), 3549—3564.

Gao, B.C., Heidebrecht, K.B., Goetz, A.F.H., 1993. Derivation of scaled surface reflectances from AVIRIS data. Remote Sensing of Environment 44, 165—178.

Gao, B.C., Davis Curtiss, O., Goetz, A.F.H., 2006. A review of atmospheric correction techniques for hyperspectral remote sensing of land surfaces and ocean colour. In: Geoscience and Remote Sensing Symposium, pp. 1979–1981.

Glorie, S., De Grave, J., Singh, T., Payne, J.L., Collins, A.S., 2014. Crustal root of the eastern Dharwar Craton. U-Pb age and Lu-Hf isotopic evolution of the east Salem block, southeast India. Precambrian Research 249, 229–246.

Goetz, A.F.H., Ferri, M., Kindel, B., Qu, Z., 2002. Atmospheric correction of Hyperion data and techniques for dynamic scene correction. In: International Geoscience and Remote Sensing Symposium (IGARSS), Toronto, Ont., vol. 3, pp. 1408–1410.

Guo, Y., Zeng, F., 2012. Atmospheric correction comparison of Spot-5 image based on model FLAASH and model QUAC. In: International Archives of the Photogrammetry, Remote Sensing and Spatial Information Sciences, vol. XXXIX-B7, XXII ISPRS Congress, 25 August – 01 September 2012, Melbourne, Australia.

Hubbard, B., Crowley, J.K., 2005. Mineral mapping on the Chilean–Bolivian Altiplano using co-orbital ALI, ASTER and Hyperion imagery: data dimensionality issues and solutions. Remote Sensing of Environment 99 (1–2), 173–186.

Hunt, G.R., 1979. Near-Infrared (1.3–2.4 m) spectra of alteration minerals potential for use in remote sensing. Geophysics 44, 1974–1986.

Kruse, F.A., Boardman, J.W., Huntigton, J.F., 2003. Comparison of airborne hyperspectral data and EO-1 Hyperion for mineral mapping. IEEE Aerospace Conference Proceedings IEEE Transactions on Geoscience and Remote Sensing 41 (6), 1388–1400.

Kurt, Simon, 2006. Hyperion Level 1G (1GST) Product Output Files Data Format Control Book (dfcb), Earth Observing-1 (EO-1).

Lau, I.C., 2004. Application of atmospheric correction to hyperspectral data: comparisons of different techniques on Hymap data. In: The 12th Australasian Remote Sensing and Photogrammetry Conference Proceedings, Fremantle, Western Australia.

Meer, F.D.V.D., Harald, M.A.V.D.W., Frank, J.A.V.R., Hecker, C.A., Bakker, W.H., Noomen, M.F., Meijde, M.V.D., Carranza, E.J.M., Smeth, J.B.D., Woldai, T., 2012. Multi- and hyperspectral geologic remote sensing. A review. International Journal of Applied Earth Observation and Geoinformation 14 (1), 112–128.

Papp, E., Cudahy, T., 2002. Hyperspectral remote sensing. In: Papp, E. (Ed.), Geophysical and Remote Sensing Methods for Regolith Exploration, CRCLEME Open File Report, vol. 144, pp. 13–21.

Rani, N., Singh, T., Mandla, R.V., 2015. Comparison of atmospheric correction of Hyperion image using FLAASH and QUAC methods. In: Rao, Madhava V., Rao, Kesava P., Kumar Phanindra, T., Murthy, D.S.R. (Eds.), Geoinformatics Applications in Rural Development. Professional Books Publisher, Hyderabad, ISBN 978-81-909728-9-5, 452–259.

Rowan, L.C., Simpson, C.J., Mars, J.C., 2004. Hyperspectral analysis of the ultramafic complex and adjacent lithologies at Mordor, NT, Australia. Remote Sensing of Environment 91, 419–431.

San, B.T., 2008. Hyperspectral Image Processing of EO-1 Hyperion Data for Lithological and Mineralogical Mapping. Ph. D. Thesis. METU, Department of Geological Engineering, p. 142.

USGS, 2004. EO-1, User Guide Version 2.3.

Van der Meer, F.D., De Jong, S.M., 2001. Imagining Spectroscopy: Basic Principles and Prospective Applications, vol. 4. Springer Science & Business Media, pp. 3–16.

Van Ruitenbeek, F.J.A., Debba, P., Van Der Meer, F.D., Cudahy, T., Van Der Meijde, M., Hale, M., 2006. Mapping white micas and their absorption wavelengths using hyperspectral band ratios. Remote Sensing of Environment 102, 211–222.